ICARUS **123,** 478–490 (1996)
ARTICLE NO. 0173

Stellar Occultation by 2060 Chiron

SCHELTE J. BUS

Department of Earth, Atmospheric and Planetary Sciences, Massachusetts Institute of Technology, Cambridge, Massachusetts 02139-4307; and Lowell Observatory, 1400 West Mars Hill Road, Flagstaff, Arizona 86001-4499
E-mail: sjb@astron.mit.edu

MARC W. BUIE AND DAVID G. SCHLEICHER

Lowell Observatory, 1400 West Mars Hill Road, Flagstaff, Arizona 86001-4499

WILLIAM B. HUBBARD, ROBERT L. MARCIALIS, AND RICHARD HILL

Lunar and Planetary Laboratory, University of Arizona, Tucson, Arizona 85721

LAWRENCE H. WASSERMAN, JOHN R. SPENCER, ROBERT L. MILLIS, OTTO G. FRANZ, AND AMANDA S. BOSH

Lowell Observatory, 1400 West Mars Hill Road, Flagstaff, Arizona 86001-4499

EDWARD W. DUNHAM AND CHARLES H. FORD

Space Science Division, NASA Ames Research Center, Moffett Field, California 94035-1000

JAMES W. YOUNG

Table Mountain Observatory, JPL/Caltech, P.O. Box 367, Wrightwood, California 92397-0367

J. L. ELLIOT

Department of Earth, Atmospheric, and Planetary Sciences, Massachusetts Institute of Technology, Cambridge, Massachusetts 02139-4307; and Lowell Observatory, 1400 West Mars Hill Road, Flagstaff, Arizona 86001-4499

AND

RICHARD MESEROLE, CATHERINE B. OLKIN, STEPHEN W. MCDONALD, JEFFREY A. FOUST, LISA M. SOPATA, AND REBA M. BANDYOPADHYAY

Department of Earth, Atmospheric, and Planetary Sciences, Massachusetts Institute of Technology, Cambridge, Massachusetts 02139-4307

Received February 6, 1995; revised March 11, 1996

A 14th magnitude double star was occulted by 2060 Chiron on 1993 November 7. Observations of this event were obtained from five locations in California. An occultation by Chiron's nucleus was recorded at one of these sites, while a possible graze by the nucleus was seen at the next closest location. If this possible graze represents a true detection of the nucleus, Chiron's radius is determined to be 89.6 ± 6.8 km, assuming a circular outline for the shape. If the nucleus was not seen at the second location, Chiron's radius is only constrained as being greater than 90.2 ± 6.5 km. The presence of dust in Chiron's inner coma was also detected in four of the five occultation datasets. Lightcurve features were identified that may be explained by narrow, collimated jets of material, and by a much larger region of dust distributed asymmetrically about Chiron's nucleus. Periodic fluctuations in the dust may have been detected in one of the lightcurves. If this periodicity is real, and is induced as a result of Chiron's rotation, then a minimum expansion velocity for the dust is found to be ~40 m sec^{-1}.

INTRODUCTION

Interest in the unusual Solar System object 2060 Chiron has continued to grow since its discovery in 1977 (Kowal 1979). While early physical studies of this object concentrated on photometric properties, such as its color and

0019-1035/96 $18.00

rotational lightcurve (e.g., Hartmann *et al.* 1981, Bus *et al.* 1989), much of what we can infer about Chiron's physical nature has resulted from observations of its cometary behavior. These observations have been well documented, beginning with the report by Tholen of an unexpected brightening of Chiron in 1988 (Hartmann *et al.* 1990). A dust coma was first detected in 1989 by Meech and Belton (1990) and has been regularly observed since, including in late 1992 when Marcialis and Larson (1993) reported observing a tail. Evidence for gaseous emission has also been reported, based on the detections of CN (Bus *et al.* 1991) and CO (Womack and Stern 1995).

A basic property of Chiron which is not well determined is its size. Many conclusions about Chiron's observed behavior are based on assumptions concerning its large size, or more importantly, its mass. In particular, the formation and development of Chiron's coma must be influenced by self-gravity, an effect usually ignored in the study of smaller comets. Some fraction of the dust ejected from active regions probably does not escape Chiron, leading to substantial resurfacing of the nucleus. Dust particles which attain the appropriate velocity may be injected into quasi-stable orbits around Chiron, though the likelihood of a substantial bound coma has been debated (Meech and Belton 1990, Jewitt 1993, Stern *et al.* 1994).

To determine the size of its nucleus, several radiometric observations of Chiron have been attempted. The first thermal infrared observation was made in 1983 by Lebofsky *et al.* (1984), who obtained a tentative 2σ measurement at 22.5 μm. Using the standard thermal model, a nominal radius of 90 $+20/-25$ km ($\leq$125 km at the 2σ level) was derived. Sykes and Walker (1991) determined an upper limit to Chiron's radius of 186 km by reanalyzing the 1983 results of Lebofsky *et al.* and including the nondetection of Chiron by the Infrared Astronomical Satellite. A nondetection at 800 μm led Jewitt and Luu (1992) to place a 3σ upper limit on Chiron's radius of 150 km. Most recently, a series of measurements obtained at both 10 and 20 μm was reported by Campins *et al.* (1994) from which a color temperature was derived, and a mean value of 90 km was found for Chiron's radius. In each of these observations, the contribution from the dust coma to the thermal flux is uncertain. However, the consistency between the radius of Chiron determined in 1983 by Lebofsky *et al.* and the values found more recently by Campins *et al.* seems to indicate that the thermal contribution due to dust may be minimal.

Stellar occultation measurements potentially provide a more direct method for determining the size of Chiron. An effort was begun in 1992 to identify future occultations by Chiron (Bus *et al.* 1994) with the intention of mounting coordinated observing campaigns for the more promising events. Results from the first such occultation, of a star we designated Ch02, are reported here. A subsequent occultation by Chiron of the star Ch08 has also been observed. Results from that event (Elliot *et al.* 1995) include high signal-to-noise detections of jet-like structures in the vicinity of Chiron. A broad, tenuous distribution of material was also revealed that may be consistent with a gravitationally bound coma, but an occultation by the nucleus was not observed.

PREDICTION AND ASTROMETRY

An occultation of the 14th magnitude star Ch02 (GSC 249 00971) by Chiron was first predicted by Bus *et al.* (1994) to be observable from northern California and Nevada. Refinements to this prediction were made over the course of 2 weeks prior to the occultation using CCD images obtained at the prime focus of the 0.9-m Crossley reflector at Lick Observatory. These observations were made with a camera derived from the SNAPSHOT camera design (Dunham *et al.* 1985), but using a single Ford/Loral 2048 square front-illuminated CCD. Operated in strip-scan mode (Dunham *et al.* 1994), this system provided nightly measurements of Chiron's position relative to that of Ch02. Strip-scan images obtained each night were transferred via FTP to the Massachusetts Institute of Technology for rapid astrometric analysis (Olkin and Elliot 1994), which led to daily refinements of the shadow track prediction.

A total of 141 strip-scan exposures were obtained for astrometry from 1993 October 28 until 1993 November 08. Due to Chiron's motion in declination, it was possible to image Chiron and Ch02 together within a single strip scan only during November 2–8. Based on the earliest strip-scan astrometry, the predicted shadow track was located as far north as Idaho. After November 2, the prediction began to shift southward, and just 2 days before the event, the nominal centerline was located well into Mexico. However, the final astrometric observations obtained prior to the occultation indicated that the shadow track would be farther north, and put the centerline in the southernmost part of California. These large variations in the strip-scan predictions are now understood to arise from higher-order field distortions across the focal plane of the Crossley reflector (Dunham *et al.* 1994). With the uncertainty in the location of the shadow track, and the complicated customs formalities that would have been required, the portable field stations were not moved across the Mexican border. Our final deployment strategy was to provide approximately 45-km cross-track spacings between observing sites, with the southernmost site essentially on the border with Mexico.

A final astrometric solution based on all strip scans, including those obtained the night after the occultation, gives a geocentric impact parameter of $+0.261 \pm 0.029$ arcsec, with minimum separation occurring on 1993 November 7 at 13:18:24 Universal Time. This corresponds

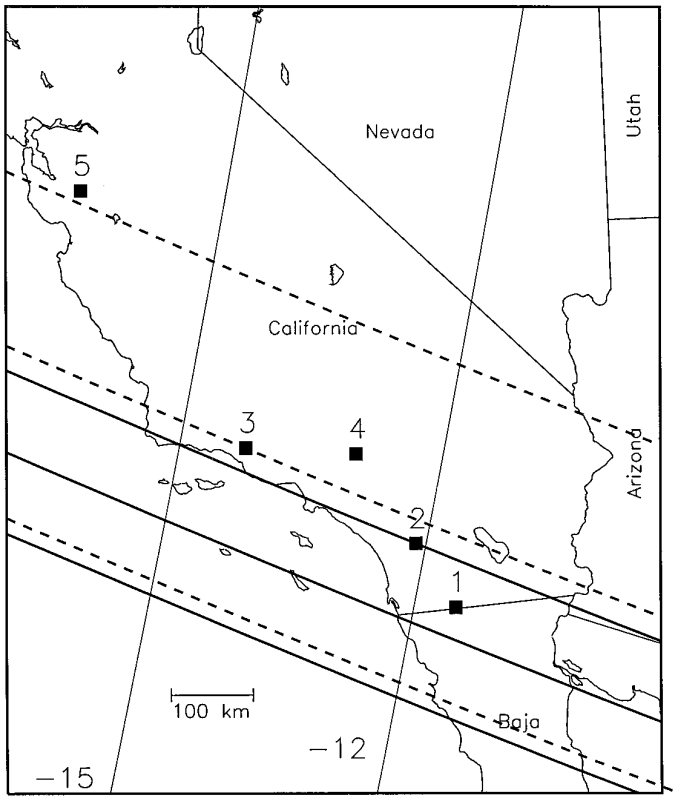

FIG. 1. Plot of the inferred shadow track of 2060 Chiron. The three dark lines running predominately east–west are the northern limit, centerline, and southern limit of Chiron's shadow, as inferred from the occultation results. The thinner, nearly north–south lines show the locations where the Sun elevation was −15° and −12° at 1993/11/07 13:15:30 UT, about the time Chiron's shadow crossed the coast. The dashed lines show the final predicted centerline and the $\pm 1\sigma$ centerlines for the occultation, determined from the strip-scan astrometry. The locations of the five observing sites are indicated by square symbols.

to a shadow track centerline which passes just north of Los Angeles and a cross-track uncertainty in the prediction of 194 km. In Fig. 1, the three dashed lines show the position of the predicted centerline and the $\pm 1\sigma$ uncertainties in this prediction. Also shown are the locations of our observing sites and the actual shadow track (heavy solid lines) as inferred from the occultation observations which we describe below.

OBSERVATIONS

The predicted shadow path and time for the occultation put strong constraints on the selection of observing sites, with the California coastline defining the western limit, twilight providing the eastern limit, and the border with Mexico defining the southern limit. At the time of the occultation, a 47% illuminated Moon was just 19° west of Ch02 in the sky, but this had little effect on the observations compared to the increase in sky brightness with morning twilight. Observations were obtained from five locations: Tierra del Sol (site 1), Palomar Mountain Observatory (site 2), Ojai (site 3), Table Mountain Observatory (site 4), and Lick Observatory (site 5). The planned distribution of observing locations called for sites 1 and 2 to be closer to the southern coastline of California. However, low coastal clouds and smoke from forest fires forced these observing teams to choose sites farther inland and at higher elevation. Details about the observing sites, and the data obtained from each, are given in Table I.

Portable occultation systems were deployed to sites 1, 2, and 3. Each system included a 0.35-m reflector and a CCD camera capable of image readout rates of up to 8 Hz (Buie *et al.* 1993a). The cameras were produced by Photometrics and use a thermoelectrically cooled 576 × 384 Thompson 7883 CCD. An optical coupling unit was used in mounting the camera to the telescope and provided 1:1 reimaging optics. No filter was used, allowing the full sensitivity range of the CCD to be utilized. The occultation data were taken in frame-transfer mode, in which a continuous series of observations are recorded with no deadtime between successive images. In this configuration, extra sky signal accumulated in the time between the frame transfer and the readout of the array, such that proper flat field images could not be obtained. Fortunately, the use of 1:1 reimaging optics and the intrinsic uniformity of the CCDs meant that flat fielding could be omitted. A series of dark frames were obtained with each system, and were applied as part of the data reduction.

Site 4 used the 0.6-m reflector at Table Mountain Observatory, with a CCD camera system identical to those used at sites 1–3. Due to the greater image scale, 3:1 reduction optics were used, again with no filter. Observations at site 5 were obtained with the 0.9-m Crossley reflector at Lick Observatory. The same CCD camera used for the astrometric strip scans was used to take a series of unfiltered occultation images in frame-transfer mode. Dark frames and flat field images were obtained in conjunction with the site 5 occultation data, but could not be used in the reductions.

The topographic locations of the observing stations were determined by TRAK 8820-1 GPS receivers using the WGS84 reference datum. These receivers also provided a precise time source against which the observations could be referenced. However, sites 1 and 3 did not achieve the full timing accuracy possible. The observations obtained at site 1 were precisely triggered by the 1-Hz GPS pulses, but the start time of the occultation sequence was not accurately recorded. A start time for the site 1 data was reconstructed from the internal DOS computer clock and the time at which the data file was written, but this start time could be incorrect by exactly one or more integer seconds. At site 3, a cable failure prevented all GPS signals

TABLE I
Observation Summary

Location	Site 1 Tierra del Sol	Site 2 Mt. Palomar	Site 3 Ojai	Site 4 Table Mtn.	Site 5 Mt. Hamilton
Observers	Marcialis Hill	Bus Meserole	Wasserman Spencer	Dunham Buie	Ford
West Long.	+116:20:00.5	+116:51:45.2	+119:13:21.4	+117:40:55.3	+121:38:38.9
Latitude	+32:36:49.2	+33:21:14.5	+34:26:39.7	+34:22:53.0	+37:20:17.8
Altitude	1135 m	1691 m	258 m	2288 m	1251 m
Distance to Centerline					
Ch02-A	28 km	83 km	110 km	156 km	318 km
Ch02-B	255 km	310 km	337 km	383 km	545 km
Time Shift relative to Ch02-A/Site 1					
Ch02-A	0.0 sec	−2.4 sec	−10.9 sec	−5.9 sec	−20.0 sec
Ch02-B	8.1 sec	5.7 sec	−2.8 sec	2.2 sec	−11.9 sec
Tele. Aper.	0.35 m	0.35 m	0.35 m	0.6 m	0.9 m
Image Scale	2.5 ″/pix	2.5 ″/pix	2.5 ″/pix	1.5 ″/pix	1.2 ″/pix
UT Start	13:07:49	13:05:01	13:12:01	13:03:01	13:06:59
UT End	13:19:29	13:25:01	13:29:47	13:23:01	13:42:59
Exp. Time	2.0 sec	1.5 sec	1.5 sec	1.0 sec	2.0 sec

from reaching the control computer. Instead, the integrations were controlled by an internal system clock. The absolute time and integration interval were determined from pulses introduced into the data stream by shining a flashlight into the telescope at known times.

REDUCTIONS

The Ch02 occultation was one of the earlier field tests of the CCD systems that were deployed to sites 1–4. Due to the faintness of Ch02, observations at the highest time resolution were not practical. Instead, longer integrations were used to balance between time resolution and the signal-to-noise ratio obtained in a single data frame. Even so, the Ch02 observations pushed the limits of the portable CCD systems. Fortunately, the field immediately surrounding Ch02 contains three other stars that were recorded in the data obtained at all the sites except site 3. The positions and Johnson/Kron–Cousins magnitudes of these stars are given in Table II. Because these field stars were recorded simultaneously with Ch02 in the CCD images, they proved invaluable in both the calibration and interpretation of the occultation data.

TABLE II
Ch02 and Field Stars

Star	comment	R	$(V-R)$	R.A. (J2000)	Dec.
Chiron		15.94	0.36		
Ch02		13.69	0.62	10:28:08.02	+03:30:35.6
Star A	(bright)	9.53	0.45	10:28:14.79	+03:32:05.4
Star B	(PSF)	12.69	0.35	10:28:14.72	+03:31:04.8
Star D	(faint)	14.04	0.31	10:28:10.40	+03:30:49.9

The occultation data obtained at sites 1–3 revealed an important instrumental effect: star images recorded at each of these sites showed distortions in both their shape and their position. This effect was most noticeable in the faintest star images, and is thought to be due to poor parallel charge-transfer efficiency (CTE) of the Thompson CCDs when read out in frame-transfer mode. To understand how poor CTE might affect the resulting occultation lightcurves, data from four of the sites were independently reduced using two different methods. First, synthetic aperture photometry was performed on all five datasets and led to the initial announcement of the occultation by Buie *et al.* (1993b). Subsequently, the datasets from sites 1, 2, 4, and 5 were reexamined using a numerical point-spread-function (PSF) technique.

Aperture Photometry Reductions

The occultation data obtained at each site were first corrected for bias and dark counts. Flat field calibrations were applied only to the data from site 4, due to the use of 3 : 1 reduction optics. The systems used at the other sites produced images that were found to be sufficiently flat and required no further calibration. Instrumental fluxes were then obtained for each star image by synthetic aperture photometry, using the same algorithm and software described by Buie and Bus (1992). An initial pass through each dataset was used to find centroided locations for the stars on all of the occultation images. From these positions,

the mean offset of each field star relative to star A was computed. In a final pass through the data, the aperture locations were determined by adding these mean offsets to the position of star A on each frame. An object aperture radius of 5 pixels was used in the reduction of all of the datasets.

The final step in creating the occultation lightcurves for Ch02 was to remove the contribution of Chiron from the combined flux measured in the blended images. The flux ratio of Chiron/Ch02 was determined to be 0.1364 ± 0.0010 a few hours before the occultation from stare mode images obtained at site 4. Due to the small amplitude of Chiron's rotational lightcurve (Marcialis and Buratti 1993), any change in this ratio in the hours leading up to the occultation was expected to be small ($<1\%$). Once the contribution of Chiron was subtracted, the corrected Ch02 flux was divided by the combined average flux of the other stars on the frame. The resulting lightcurves were finally normalized assuming that Ch02 remained unocculted during the interval from 13:07 to 13:12 UT. In the case of site 3, no field stars were measured, so the final lightcurve consists of the raw Ch02 measurements, corrected for the flux contribution from Chiron, and normalized over the interval from 13:21 to 13:25 UT.

Numerical PSF Reductions

Data from sites 1, 2, 4, and 5 were reexamined using the technique of numerical PSF model fitting. In this technique (Elliot *et al.* 1995), the nominal PSF model is derived from one or more stars in an image. This model can be fitted to other stars in the image, often resulting in improved signal-to-noise over standard aperture photometry.

The preprocessing of each dataset was almost identical to that used for the aperture reductions, with the same dark and flat field procedures being applied. A row-by-row background subtraction was then performed on each image, resulting in a median background level of zero. The image of star B was defined to be the point-spread function for each frame and was fitted to the blended image of Ch02 and Chiron using a two-source model. In the fit, Chiron's position was fixed with a known pixel offset from Ch02. The flux contribution from Chiron was also fixed, based on measurements of the relative brightnesses of Chiron and star B obtained at site 4 just 2 hr before the occultation. The PSF was also fitted to star D, providing a check of the reduction process. The lightcurves produced using this technique are in the form of a flux ratio and were normalized using the same time intervals as those used in the aperture reductions.

These lightcurves were examined for possible correlations between the measured flux ratio and position of the star image on the CCD. Telescope tracking errors and guiding corrections made during the observations resulted in the star positions shifting over many pixels. Since four of the five datasets were not flat fielded, variations in the measured flux might be related to changes in the position of an image across the CCD. While some correlation with position was found in each occultation dataset, it was not statistically significant and contributed little to the appearance of the lightcurves.

DESCRIPTION OF THE OCCULTATION LIGHTCURVES

The final normalized lightcurves resulting from the two reduction techniques are shown in Figs. 2 and 3. In Fig. 2, all of the data obtained between 13:03 and 13:25 UT are plotted at full time resolution. Figure 3 shows only those data taken between 13:15 and 13:16.4 UT, along with the error associated with each point. Each lightcurve has been shifted in time to match that of site 1, correcting for the relative along-track locations of the different observing sites.

Many low-level fluctuations are seen in the lightcurves, especially in those from sites 1, 2, and 3, where the signal-to-noise of the data is low. Any variation in the level of these lightcurves that we attribute to the presence of Chiron must be physically plausible. In particular, if they are caused by regions of material in the vicinity of Chiron, these features should be traceable from one lightcurve to the next. A careful examination of the data shows that only a few features, centered around the time of the predicted occultation, can be seriously attributed to Chiron's passage in front of Ch02.

The most prominent lightcurve feature appears in the observations from site 1, where a sharp drop in the brightness of Ch02, lasting about 7 sec, can be seen centered at 13:15:39.5 UT. This feature is labeled A1 in Fig. 3, and is assumed to be the result of an occultation by the nucleus. Also present is an asymmetric depression surrounding the nuclear event, extending from approximately 13:14.2 to 13:17.7 UT as measured from the PSF lightcurve. The extent of this depression is labeled B1 in Fig. 2.

The lightcurves from site 2 show a single low point, labeled A2, which is approximately coincident in time with the central occultation recorded at site 1. When an offset of +1 sec is applied to the site 2 data, the minima in the two datasets can be aligned almost exactly. This offset is consistent with the uncertainty in the start time for the site 1 dataset. A broad depression, labeled B2, is seen in the PSF-reduced lightcurve, extending from 13:14.8 to 13:16.7 UT.

Large variations are present in the level of the site 3 lightcurve which cannot be considered significant. A single low point, A3, is noted because of its coincidence in time with point A2. The lightcurves obtained from sites 4 and

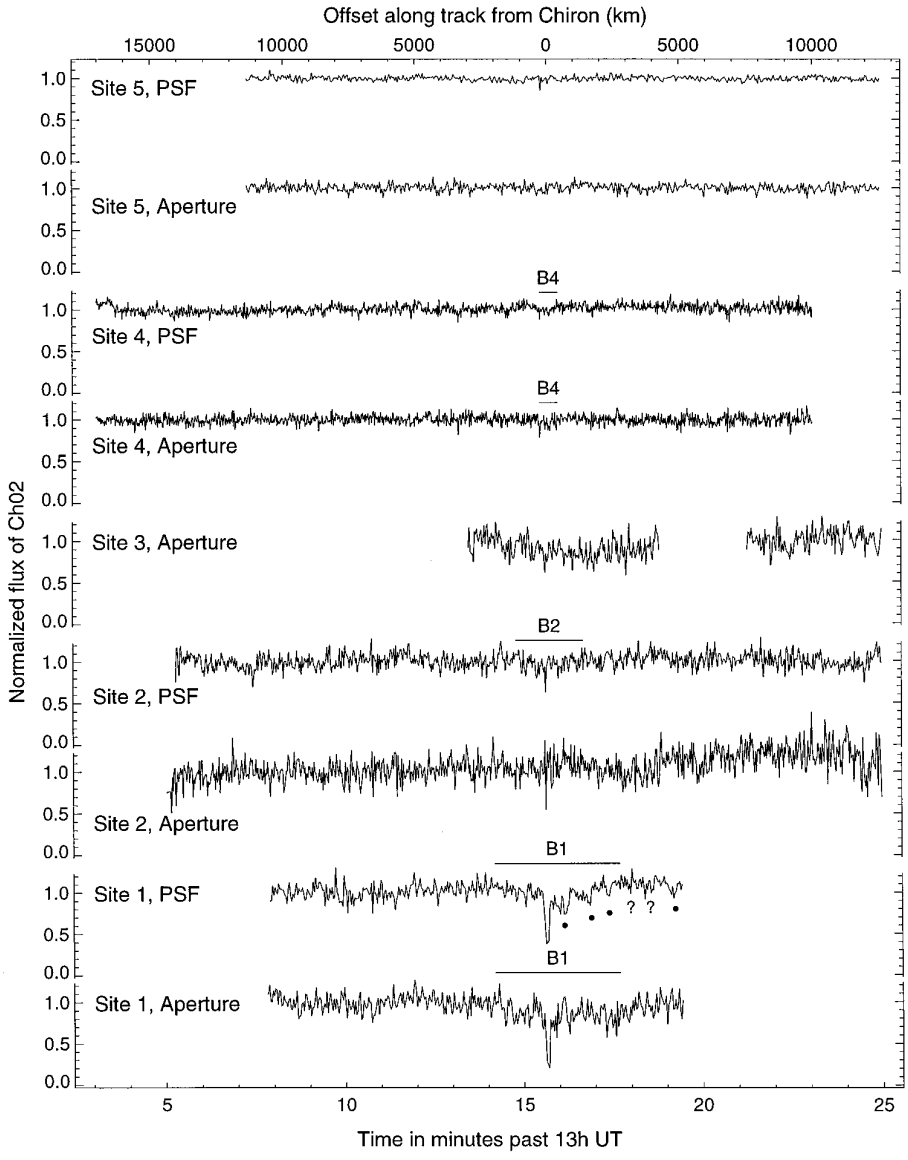

FIG. 2. Normalized Ch02 occultation lightcurves. Those lightcurves marked "Aperture" were reduced using synthetic aperture extractions, while those marked "PSF" were reduced using a point-spread-function fitting algorithm. Each lightcurve has been shifted in time to match that of site 1, correcting for the relative along-track locations of the different observing sites by the shift relative to Ch02-A/Site 1 given in Table I. Broad depressions in the lightcurves are labeled (B1, B2, and B4), and possible periodic features noted in the PSF-reduced lightcurve from site 1 are marked with a dot or a "?".

5 both have relatively high signal-to-noise, compared to the data from the other sites. No significant features are seen except for a shallow depression in the site 4 lightcurve (labeled B4) and a single point marked A4 which is centered around the predicted occultation time. A single low point also appears in the PSF-reduced lightcurve from site 5. This latter point is not seen in the aperture photometry reductions and is regarded as an artifact in the PSF lightcurve caused by an abnormally high-valued pixel in the image of Star B on a single frame.

In neither reduction of the site 1 data does feature A1 drop to the zero level, even after the light contribution of Chiron is accounted for. Several explanations for the residual flux in this occultation chord were considered, including the possibility that Ch02 is an unresolved binary star (Buie *et al.* 1993b). Initial spectroscopic observations of Ch02 revealed no obvious duplicity of the star (R. Wagner, private communication). However, on 1995 December 5 UT, observations were obtained using the Fine Guidance Sensors (FGS) on the Hubble Space Telescope which clearly show Ch02 to be a double star. Using the broadband F583W filter, the two components were found to have a

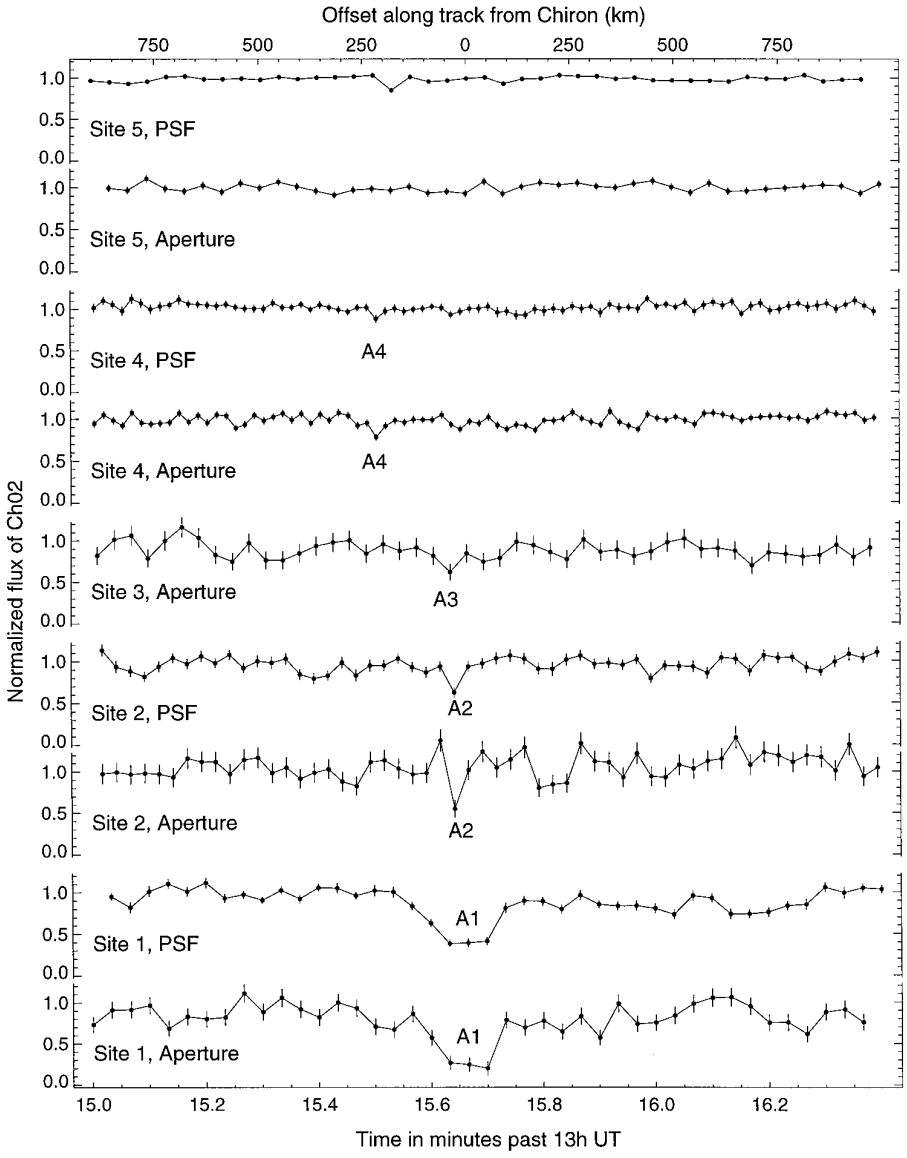

FIG. 3. Expanded Ch02 occultation lightcurves. These lightcurves are the same as those in Fig. 2, but have been expanded to show detail around the time of the central occultation. The individual data points and their uncertainties are shown. Narrow lightcurve features (A1–A4) have also been marked.

magnitude difference of 0.06 ± 0.02. The stars were separated by 0.0436 ± 0.0002 arcsec, and the fainter component (Ch02-B) was at a position angle of 67.5 ± 1.0° with respect to the brighter one (Ch02-A). The nearly equal brightness of the two stars suggests similar spectral types, so that identification of this binary from spectral observations would have been difficult. The separation and orientation of the two components in the sky define the relative separation of the two shadow tracks on the Earth. The fact that no nuclear chord is observed in the site 4 dataset implies that Ch02-A is responsible for the occultation observed at site 1, and that the shadow centerline associated with Ch02-B passed across Baja California, about 275 km south of site 1. In Table I, the perpendicular distance of each site is given with respect to the each of the shadow centerlines. The time shift along the track relative to the Ch02-A shadow as measured at site 1 is also given. These time shifts arise from the known shadow velocity, the relative position of the shadows cast by the two stars, and the separation between the observing sites in the direction of the shadow velocity.

Radius

While the sharp drop in starlight indicated by feature A1 is the result of an occultation by the nucleus of Chiron,

an explanation for the single low point observed at site 2 is not as certain. If feature A2 is interpreted as a grazing occultation of the nucleus, then we can directly solve for the size of Chiron. However, during the more recent Ch08 occultation by Chiron (Elliot *et al.* 1995), a short-lived drop in starlight, very similar in appearance to feature A2, was recorded by both the Kuiper Airborne Observatory and by an observer at the South African Astronomical Observatory. The chance of grazing the nucleus during a particular occultation is small, but doing so during each of two different occultation events is highly unlikely. A more plausible explanation may be that each of these stellar occultations sampled approximately the same region of a collimated jet of material being ejected from Chiron's surface. If this is the case, we must conclude that no chord was observed from site 2, and when combined with the site 1 data we can only place a lower bound on the radius of Chiron.

Assuming that feature A2 is a graze by the nucleus, we fitted a circular occultation model to the portions of the site 1 and site 2 lightcurves centered on the putative chords. The model included nine free parameters: the radius of Chiron, a central impact parameter, linear trends to the background levels at each site, a nonzero base level for the central occultation, an event midtime, and a timing offset between sites 1 and 2. A circular cross section for Chiron is the most complex model the observations can support, and is somewhat justified by the lack of lightcurve evidence for gross irregularities in shape (Marcialis and Buratti 1993). The model fit from the aperture photometry results gives a radius of 82.0 ± 9.6 km, whereas the numerical PSF results give a radius of 89.6 ± 6.8 km. Plots of the model fit and residuals derived from the PSF-reduced lightcurves are shown in Fig. 4.

If feature A2 represents a miss, or at best a near graze of the nucleus, then we can use the site 2 observations to place a lower bound on the radius of Chiron. Using the cross-track separation between sites 1 and 2 of 54.6 km, the site 1 chord length of 165.7 ± 8.6 km constrains the radius to be $r \geq 90.2 \pm 6.5$ km.

The radius solution, described above, allowed for a shift in the relative chord positions by introducing a fitted time offset between sites 1 and 2. The need for this offset could be used to possibly discriminate between the two interpretations of feature A2. The uncertainty in the start time at site 1 allows for shifts of an integral number of seconds, while our radius solutions require offsets of 0.75 ± 0.31 sec and 0.71 ± 0.42 sec for the PSF and aperture results, respectively. A 1-sec shift is within the error of both of these fitted values, though attempts to fit the data by forcing an exact 1-sec shift did not always converge. An offset between the lightcurve minima of 0.25 sec would imply a spatial displacement along the occultation chords of about 5 km. This could be caused by topographic irregularities

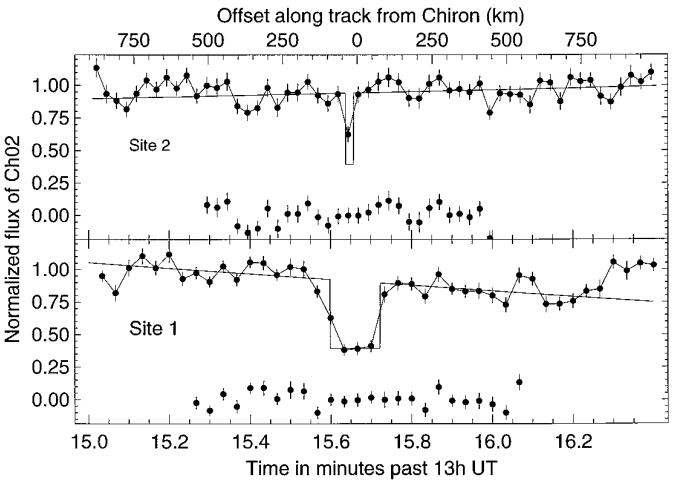

FIG. 4. Model fit for radius solution. The top graph shows the radius model fit superposed on the data from site 2, assuming that the single low point is due to an occultation chord. Below are the residuals to the fit. The bottom graph shows the fit, using the same model, to the site 1 data, where a nuclear chord was definitely observed.

encountered along the limb of Chiron during a grazing occultation. The scale of such topographic roughness is consistent with that found in the limb profiles of many icy satellites smaller than a mean radius of ~150 km (Thomas, 1989).

Narrow Dust Feature

The fact that Ch02 is a binary star must be addressed in the interpretation of the occultation lightcurves. Figure 5 depicts the Chiron-centered sky plane, showing the region of space around Chiron that was sampled by the different observing sites. Information gathered at each site resulted from the combined light of the two stars, the tracks of which are indicated on the sky plane. The occultation tracks resulting from Ch02-B all lie well to the north of Chiron. Because the lightcurve from site 5 is essentially flat, we conclude that Ch02-B does little to modify the occultation data obtained at the other sites, other than provide additional flux which must be accounted for in any quantitative analysis of the lightcurves.

If we assume that feature A2 is not the result of a graze by the nucleus, then the interpretation of a jet (Buie *et al.* 1993b) is in order. The lightcurves obtained at sites 3 and 4 also show single low points, features A3 and A4, which are nearly coincident in time with the central occultation. Though these individual points are not significant given the noise level of the respective lightcurves, the significance of their alignment must be considered. This alignment is shown, with respect to Chiron, in Fig. 5.

The 1-sec integration interval used at site 4 is useful in constraining the shape of the jet. If it is assumed that the

jet material originates from a point source on Chiron's surface, then feature A4 indicates that this material has traveled ~250 km as projected on the sky plane. The width of the lightcurve feature implies the jet is no wider than 22 km when measured along the site 4 track, yielding a cone angle <5°. This is smaller than the nominal spreading angle of 12° determined for the similar feature observed in the Ch08 results (Elliot *et al.* 1995).

A tightly collimated jet should have little mass loss as it extends outward, with the material expanding to fill the cone angle. Thus, measures of the optical depth of this structure, integrated over distance along the occultation track, should be consistent for the lightcurves from each site. The integrated optical depths were calculated using the method of Elliot *et al.* (1995), who define the averaging interval to be the product of the apparent shadow velocity and the integration interval for the data. To account for the extra flux from Ch02-B, the lightcurves were first renormalized using the depth of the nuclear occultation at site 1 to define the zero level. Values for the integrated optical depths of features A2, A3, and A4 are given in Table III and can be compared to that of 13.2 km given for the narrow feature in the Ch08 lightcurve as determined from the KAO optical data (Elliot *et al.* 1995). Features A2, A3, and A4 actually show a significant decrease in optical depth as a function of distance from Chiron, indicating that material is rapidly lost from the detectable portion of the jet. This is consistent with the lack of a similar feature being detected in the high signal-to-noise lightcurve obtained at site 5.

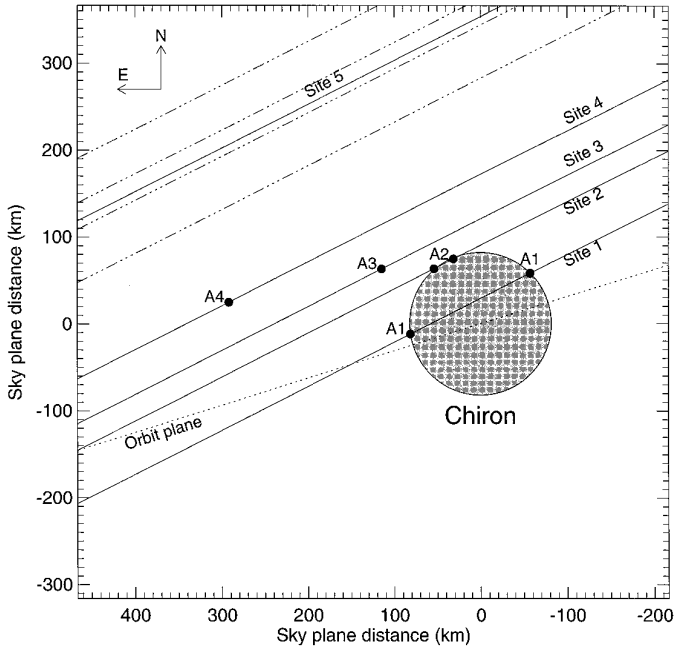

FIG. 5. Sky-plane geometry for the region immediately surrounding Chiron. The disk of Chiron is shown with a size corresponding to the radius solution that assumes a site 2 chord. The apparent track of Ch02-A is depicted for each site by a solid line and the tracks corresponding to Ch02-B are shown as dot–dashed lines. A dotted line shows the projected orbital plane of Chiron. The projected sunward vector happens to fall very close to the orbit plane, but because the phase angle was so low ($\alpha = 6°$), the true direction to the Sun is nearly out of the page. The sky-plane location of the narrow lightcurve features from Fig. 3 are also labeled (A1–A4).

It is interesting to note that the jet-like feature seen in the Ch08 occultation lightcurves occurred about 3 sec before Chiron's closest approach to the star. This puts the detected material about 50 km west of the line perpendicular to Chiron's motion, as projected on the sky plane. The jet-like feature we note in the Ch02 lightcurves appears to the east of this line. The rotation period of Chiron is well determined (Marcialis and Buratti 1993), so that in the time between the Ch02 and Ch08 occultations, Chiron made 496.5 rotations. We could speculate that the Ch02 and Ch08 features are both caused by a single jet originating from the same source region on Chiron's surface. If so, the small displacement of the jet as seen on the sky plane between the two occultations, coupled with the difference in Chiron's rotational phase, would imply that the active region is at a moderately high latitude on Chiron's surface. By the same argument, the projected orientation of Chiron's rotational pole on the sky plane would lie between the two observed locations of the jet, implying a relatively low obliquity for Chiron.

Broad Dust Features

Since the discovery of a dust coma in 1989 (Meech and Belton 1990), nonrotational variations in the absolute brightness of Chiron have been attributed to changes in its level of dust production. Images taken at site 4, just 2 hr before the occultation, showed Chiron to be well separated from Ch02 and allowed for an accurate measurement of its brightness. Using the known magnitudes of stars in the field, Chiron was measured at a V magnitude of 16.3, corresponding to $H_V = 6.2$. From the long-term brightness history of Chiron (Luu and Jewitt 1990), this value is intermediate in the range over which it has been observed and can be interpreted as a period of moderate activity. From the strip-scan images taken for the astrometric prediction, Chiron's brightness was monitored and found to be roughly constant for the 5 days leading up to the occultation. These observations give some indication of the amount of dust that may have been present, and possibly detectable, during the Ch02 occultation.

In addition to the narrow, jet-like feature described above, the Ch02 lightcurves contain many broad, low-level fluctuations. The majority of these lightcurve variations are not significant, and are probably not the result of Chiron's passage in front of Ch02. However, we suggest that the

TABLE III
Occultation Lightcurve Features

Feature	Probable cause	Time of event	width(km)	Depth	$\int \tau dx$ (km)
A1	occultation chord	13:15:35 – 13:15:44	158	—	—
A2	jet or chord	13:15:39	<34	0.4	30
A3	jet?	13:15:38	<34	0.5	18
A4	jet?	13:15:30	<23	0.7 – 0.8	5–7
B1	broad dust component	13:14:12 – 13:17:42	4700	0.7	220–1000
B2	broad dust component	13:14:48 – 13:16:42	2600	0.8	≤150
B4	broad dust component	13:15:30 – 13:16:00	680	0.8	12–40

alignment of features B1, B2, and B4 is significant, and that these shallow depressions in the lightcurve may result from extinction of starlight by dust in the immediate vicinity of Chiron's nucleus. The level at which these features should be interpreted can be estimated by comparing the results from the two different reduction techniques. The high signal-to-noise lightcurves obtained at sites 4 and 5 allowed for a solid determination of the unocculted baseline level. Thus, the reality of feature B4, and the lack of a similar feature in the site 5 data, should be regarded with some confidence. By comparison, fluctuations in the unocculted baseline levels recorded at sites 1–3 make it impossible to determine unique normalization factors for these data. The criteria by which each lightcurve was normalized, and thus how the baseline level was chosen, greatly affect any quantitative interpretation of the broad features.

Integrated optical depths were determined for features B1, B2, and B4 from both the aperture and the PSF lightcurves and are listed in Table III along with the time interval over which the integration was performed. Those points associated with features A1, A2, and A4 were first replaced with fitted values to the broad features, so that only the contribution from the broad dust component was measured. In Table III, a range of optical depths indicates the difference in values measured from the aperture photometry and PSF-reduced lightcurves. A realistic estimate of the uncertainties in these integrated optical depths is about a factor of two, even though comparison of the values from the two reduction techniques can reveal a scatter that is much larger. In any case, we find the integrated optical depths measured for the broad features to be an order of magnitude greater than that of the corresponding narrow feature observed at each site.

The PSF-reduced lightcurves from sites 1 and 2 show that the broad depressions, B1 and B2, are not centered symmetrically on the central occultation defined by features A1 and A2. It is also clear from Fig. 6 that the material being detected in the lightcurves falls off steeply to the north, perpendicular to the occultation tracks, such that there is no indication of the material in the lightcurves obtained at site 5. The material we detect near the nucleus of Chiron does not show azimuthal symmetry, and indicates a morphology quite different from the approximately spherical appearance of the outer coma seen in ground-based images (Meech and Belton 1990, Luu and Jewitt 1990, West 1991). Possible explanations for the dust distribution we observe include long-lived dust structures such as a dust trail (Sykes and Walker 1992), confined approximately to the orbit plane of Chiron, or material forming the inner core of Chiron's dust tail. Alternatively, the broad features may be caused by asymmetric outflow of material, resulting in a short-lived disk, arc, or fan, which may or may not be gravitationally bound. Observations of Chiron's inner coma obtained with the Hubble Space Telescope Planetary Camera in 1993 (Meech *et al.* 1994) revealed a radial structure at a projected distance of ~1200 km from

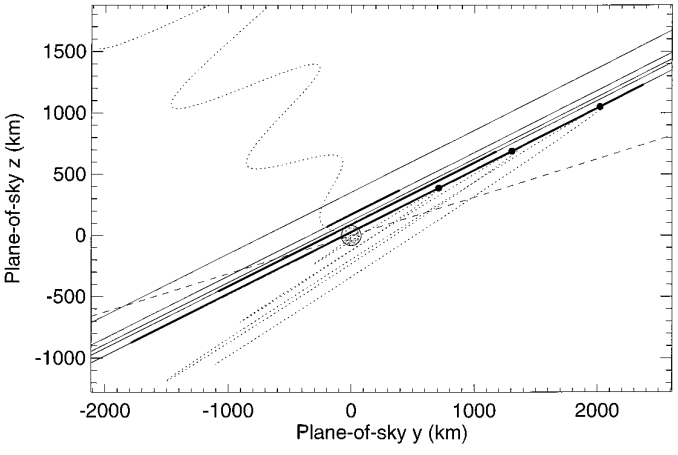

FIG. 6. Large area sky-plane geometry around Chiron. This plot is the same as Fig. 5 except for showing a larger region around Chiron. Only the tracks corresponding to the brighter component of Ch02 are shown and are not labeled for clarity. The heavy lines along these tracks mark the locations of the broad features, B1, B2, and B4. The filled circles mark the three most prominent minima in the periodic lightcurve structure. The orbit plane is indicated by the dashed line. Two spirals are drawn, depicting the geometry of two example dust jets. In this scenario, Chiron's pole is tipped 1° out of the page, 33° east of north (counter-clockwise). The ejection velocity is 36 m sec^{-1}, the equatorial jet is aimed 6° below the equatorial plane, and the polar jet is aimed 20° away from the rotation axis.

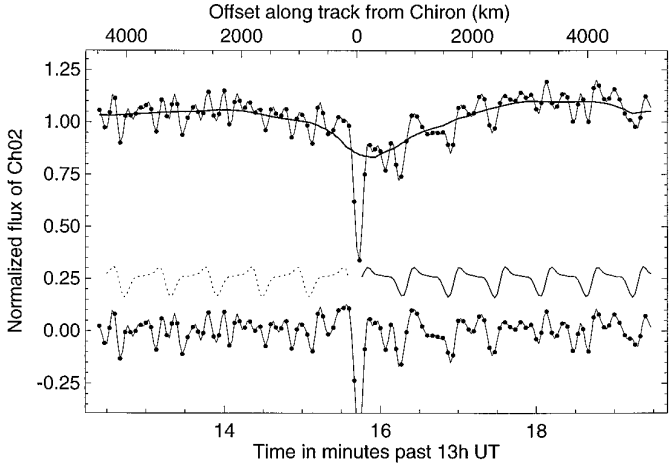

FIG. 7. Periodic lightcurve structure. At the top are the site 1 lightcurve data (connected points), filtered to a factor of two lower time resolution. These points are overlaid with a LOWESS-smoothed curve (Cleveland 1979) that follows the general shape of the broad lightcurve feature B1. These data are replotted in the bottom curve after the broad feature has been removed. In the middle is shown a periodic function, derived by phasing the data over the interval from 13:16 to 13:19:30 UT. Over this interval, the function is shown by a solid curve, representing that part of the lightcurve data where the periodicity is most pronounced. Prior to the time of the central occultation, a mirror image of the function has been shifted to provide the best fit to the data and is shown as a dotted curve.

the nucleus. Inspection of the highest signal-to-noise lightcurves obtained at sites 4 and 5 shows no detectable evidence for such a structure during the Ch02 occultation.

Periodic Structure

Examination of the PSF-reduced lightcurve from site 1 reveals a series of features that appear to repeat about every 36 sec (cf. Fig. 2). These features are most prominent over the interval from 13:16 to 13:19.5 UT, though a similar structure is visible, at a reduced level, in the 3–4 min prior to the central occultation. The periodic structure is somewhat more apparent in Fig. 7, where the site 1 lightcurve has been smoothed, reducing the time resolution by a factor of two. After the general shape of the broad feature B1 was removed, phase-dispersion minimization (PDM) (Stellingwerf 1978) was used to verify the periodicity. The periodic structure does not appear in the lightcurves from other sites and is only marginally detectable in the aperture photometry lightcurve from site 1. The reality of this periodic structure is uncertain, though no systematic effects in either the observations or the reduction of these data have been identified that could account for its presence. Likewise, it is difficult to attribute these periodic features to purely random noise.

If the periodicity observed at site 1 is real, then any plausible explanation for its presence involves some active source region on Chiron. Depending on the latitude of the source, a narrow dust jet might lead to either a disk or a cone-shaped concentration of material that could maintain a spiral record due to Chiron's rotation. The activity of the source may be continuous or fluctuate periodically, turning on and off as a result of variations in insolation caused by rotation of the nucleus. In addition, a special geometry would be required, capable of hiding the periodicity from the other occultation tracks. For example, a spiral dust cone might be oriented such that the site 1 track sampled one edge of the cone, as projected on the sky plane, with no material being detected at the other sites.

The time between each periodic cycle in the site 1 lightcurve corresponds to a distance of about 800 km projected on the sky plane. Chiron's rotation period of 5.9 hr would thus imply a minimum expansion velocity for the dust of about 40 m sec^{-1}. This value for the dust velocity is considerably higher than that of 5 ± 1 m sec^{-1} determined by Fulle (1994) for dust grain diameters of 40 μm. Although the lightcurve features are noisy, the interval between adjacent cycles in the periodic structure appears to be constant. This implies that over the range where these features are visible, about 800 to 4800 km from Chiron projected on the sky plane, no measurable change in the dust velocity is indicated. Using a radius of 90 km for the nucleus, the material associated with this periodic structure cannot be gravitationally bound to Chiron, even if we assume an unreasonably high density of 3000 kg m^{-3} for the nucleus.

Two conic, spiral jets are depicted in Fig. 6, one originating from a polar source region on Chiron and the other from a more equatorial source. These two curves are meant to illustrate one possible geometric configuration that is consistent with the observed lightcurve features, and in the case of the equatorial jet, help to demonstrate a possible geometry that explains the periodic structure. It is apparent from Fig. 6 that the nature of the two jets observed during the Ch02 occultation is very different. The polar jet identified by lightcurve features A2, A3, and A4 must have a high dispersion rate, since it was not detected in the site 5 lightcurves, and presumably decays away in less than one Chiron rotation. The equatorial jet identified by the periodic structure would have had to survive for three to six rotations with little dispersion. In fact, the apparent lack of degradation in the periodic features with distance from Chiron indicates a velocity dispersion of <2 m sec^{-1} for material within this jet.

CONCLUSIONS

The results presented here document the first attempt to examine Chiron using the stellar occultation technique. Data were obtained from five observing sites on 1993 November 7 UT, when Chiron occulted the star Ch02 (GSC 249 00971). From these data, conclusions can be drawn

about Chiron's size and about the apparent distribution of dust within Chiron's inner coma.

A clear occultation by the nucleus of Chiron was recorded at the southernmost observing location (site 1), while a less certain graze by the nucleus may have been detected at site 2. If both of these detections resulted from an occultation by the nucleus, the radius of a circular cross section through Chiron is determined to be 89.6 ± 6.8 km. If site 2 did not record a graze by the nucleus, the single chord obtained at site 1 is then used to constrain Chiron's radius to be $r \geq 90.2 \pm 6.5$ km. These values for Chiron's size are in good agreement with those determined from thermal IR measurements (Lebofsky *et al.* 1984, Campins *et al.* 1994). During the nuclear occultation, the flux from Ch02 did not drop to zero, leading to an early suggestion that the occulted star might be binary (Buie *et al.* 1993b). The duplicity of Ch02 was recently proven in follow-up observations obtained with the Hubble Space Telescope, in which the measured separation, orientation, and magnitudes of the two components are found to be consistent with the constraints placed on Ch02 as a result of the Chiron occultation.

Evidence for dust in Chiron's inner coma was seen in four of the five occultation datasets. Lightcurve features were identified which suggest the existence of both a narrow, collimated jet of material and a much larger asymmetric distribution of dust. A possible series of periodic features is also noted in one of the lightcurves.

The broad, asymmetric dust distribution detected in Chiron's inner coma during the Ch02 occultation appears to be quite different from the larger, nearly spherical dust coma seen in ground-based images. It is also significantly different than the radial structure observed in the inner coma by Meech *et al.* (1994) using the Hubble Space Telescope. These observations suggest that the occultation technique is sensitive to a population of dust particles different from that regularly observed in Chiron's coma by reflected sunlight. Possible cometary structures which might explain the broad lightcurve features include the core of a cometary tail, a dust trail confined approximately to Chiron's orbit plane, or a disk- or fan-shaped concentration of dust. It is impossible to determine what fraction of the dust particles seen in the occultation lightcurves might be gravitationally bound to Chiron on short-lived, ballistic trajectories. However, the lack of azimuthal symmetry in the dust distribution indicates that this material is not in long-lived, quasi-stable orbits around Chiron, and cannot be considered part of a bound atmosphere such as that proposed by Meech and Belton (1990). A broad, low optical-depth feature was identified in the Ch08 results (Elliot *et al.* 1995) that, based on its symmetric appearance, is consistent with a gravitationally bound coma. However, this tenuous feature would not have been detectable in the lower signal-to-noise Ch02 data. The fact that the more extensive, asymmetric structure recorded during the Ch02 event is not seen in the Ch08 results may indicate temporal variations in the distribution of dust probed by the occultation technique.

A relatively narrow dust jet appears to extend northeast of Chiron. This feature is very similar to one detected by Elliot *et al.* (1995) during the Ch08 occultation. However, evidence of this jet is not seen in the high signal-to-noise data obtained from site 5, leading to the conclusion that material may be rapidly lost from the detectable core of this jet. A second active source region on Chiron is inferred from periodic features that may be present in the lightcurve from site 1. If this periodic structure is real, and is caused by fluctuations in the distribution of dust near Chiron, then any explanation for its presence must include a special geometry capable of hiding the periodicity from the other, more northern observing sites. This very fact raises suspicion about the physical reality of these features, though no systematic effects have been identified in either the observations or the reduction of these data that could account for the periodicity. If it is assumed that the periodic structure is induced as a result of Chiron's rotation, then the dust associated with these features is found to have a minimum expansion velocity of 40 m sec^{-1} over the range that the features were observed, and indicates that the material associated with this structure is not gravitationally bound to Chiron. This apparent periodic structure is the most intriguing but least confident finding from the occultation.

While many of the conclusions drawn about Chiron as a result of the Ch02 and Ch08 occultations are not definitive, the results show the potential power of this technique for studying Chiron and other small solar system objects. Due to Chiron's small size and its distance from the Earth, the Ch02 and Ch08 events represent some of the most difficult occultation predictions ever attempted. We have shown that with a focused effort of astrometric predictions and the ability to rapidly deploy observers and equipment to the shadow track, observations such as these are feasible. Future occultations by Chiron need to be attempted to fully address the question of its size and to place better constraints on the distribution of dust in its inner coma.

ACKNOWLEDGMENTS

Our deepest thanks to Frank Santore of the San Diego Astronomical Association and to Bob Thicksten of Palomar Mountain Observatory. Each provided an observing site at a moment's notice for those of us desperately seeking clear skies on the night of the occultation. We are also deeply indebted to the HST High Speed Photometer Team, who provided instrument time in obtaining the FGS observations of Ch02. Thanks also to Mike Belton and Dave Jewitt for their very helpful comments and suggestions as referees of the manuscript. This project benefitted from NASA Planetary Astronomy Grant support for Hubbard (NAGW-1555); Elliot (NAGW-1494); Millis, Buie, Wasserman, and Spencer (NAGW-1912); and Schleicher (NAGW-3884). NSF Grants to

Lowell Observatory (AST-9121473) and MIT (AST-9120099) provided support for building the portable occultation systems used at two of the observing sites. The HST observations were supported by HSP GTO Grant NASG5-1613 (Univ. of Wisconsin). Software used in the analysis of the HST observations was developed for the HST Astrometry Team under NASA Grant NAG5-1603 (Univ. of Texas).

REFERENCES

Buie, M. W., and S. J. Bus 1992. Physical observations of (5145) Pholus. *Icarus* **100,** 288–294.

Buie, M. W., R. L. Millis, L. H. Wasserman, J. L. Elliot, S. J. Bus, E. W. Dunham, E. F. Young, W. B. Hubbard, D. M. Hunten, and W. K. Wells 1993a. CCD camera occultation system. *Bull. Am. Astron. Soc.* **25,** 1115.

Buie, M. W., C. Olkin, S. McDonald, C. Ford, J. Foust, L. Sopata, J. L. Elliot, R. L. Marcialis, S. J. Bus, R. Meserole, L. H. Wasserman, J. R. Spencer, E. W. Dunham, J. Young, T. H. Jarret, C. A. Beichmann, and T. Herter 1993b. (2060) Chiron. *IAU Circ.* **5898**.

Bus, S. J., E. Bowell, A. W. Harris, and A. V. Hewitt 1989. 2060 Chiron: CCD and electronographic photometry. *Icarus* **77,** 223–238.

Bus, S. J., M. F. A'Hearn, D. G. Schleicher, and E. Bowell 1991. Detection of CN emission from (2060) Chiron. *Science* **251,** 774–777.

Bus, S. J., L. H. Wasserman, and J. L. Elliot 1994. Chiron stellar occultation candidates: 1993–1996. *Astron. J.* **107,** 1814–1824.

Campins, H., C. M. Telesco, D. J. Osip, G. H. Rieke, M. J. Rieke, and B. Schulz 1994. The color temperature of (2060) Chiron: A warm and small nucleus. *Astron. J.* **108,** 2318–2322.

Cleveland, W. S. 1979. Robust locally weighted regression and smoothing scatterplots. *J. Am. Statistical Assoc.* **74,** 829–836.

Dunham, E. W., R. L. Baron, J. L. Elliot, J. V. Vallerga, J. P. Doty, and G. R. Ricker 1985. A high-speed, dual-CCD imaging photometer. *Publ. Astron. Soc. Pacific* **97,** 1196–1204.

Dunham, E. W., C. H. Ford, R. P. S. Stone, S. W. McDonald, C. B. Olkin, and J. L. Elliot 1994. Occultation predictions using CCD strip-scanning astrometry. *Bull. Am. Astron. Soc.* **26,** 1154.

Elliot, J. L., C. B. Olkin, E. W. Dunham, C. H. Ford, D. K. Gilmore, D. Kurtz, D. Lazzaro, D. M. Rank, P. Temi, R. M. Bandyopadhyay, J. Barroso, A. Barucci, A. S. Bosh, M. W. Buie, S. J. Bus, C. C. Dahn, D. W. Foryta, W. B. Hubbard, D. F. Lopes, R. L. Marcialis, S. W. McDonald, R. L. Millis, H. Reitsema, D. G. Schleicher, B. Sicardy, R. P. S. Stone, and L. H. Wasserman 1995. Jet-like features near the nucleus of 2060 Chiron. *Nature* **373,** 46–48.

Fulle, M. 1994. Spin axis orientation of 2060 Chiron from dust coma modeling. *Astron. Astrophys.* **282,** 980–988.

Hartmann, W. K., D. P. Cruikshank, J. Degewij, and R. W. Capps 1981. Surface materials on unusual planetary object Chiron. *Icarus* **47,** 333–341.

Hartmann, W. K., D. J. Tholen, K. J. Meech, and D. P. Cruikshank 1990. 2060 Chiron: Colorimetry and cometary behavior. *Icarus* **83,** 1–15.

Jewitt, D. 1993. Summary and discussion of observations. In *Workshop on the Activity of Distant Comets* (W. F. Huebner, H. U. Keller, D. Jewitt, J. Klinger, and R. West, Eds.), pp. 74–75. Southwest Research Institute, San Antonio, TX.

Jewitt, D., and J. Luu 1992. Submillimeter continuum observations of 2060 Chiron. *Astron. J.* **104,** 398–404.

Kowal, C. T. 1979. Chiron. In *Asteroids* (T. Gehrels, Ed.), pp. 436–439. Univ. of Arizona Press, Tucson.

Lebofsky, L. A., D. J. Tholen, G. H. Rieke, and M. J. Lebofsky 1984. 2060 Chiron: Visual and thermal infrared observations. *Icarus* **60,** 532–537.

Luu, J. X., and D. C. Jewitt 1990. Cometary activity in 2060 Chiron. *Astron. J.* **100,** 913–932.

Marcialis, R. L., and B. J. Buratti 1993. CCD photometry of 2060 Chiron in 1985 and 1991. *Icarus* **104,** 234–243.

Marcialis, R. L., and S. M. Larson 1993. Deep CCD imaging and photometry of 2060 Chiron during the 1992–1993 apparition. *Bull. Am. Astron. Soc.* **25,** 1057.

Meech, K. J., and M. J. S. Belton 1990. The atmosphere of 2060 Chiron. *Astron. J.* **100,** 1323–1338.

Meech, K. J., M. W. Buie, N. Samarasinha, B. E. A. Mueller, and M. J. S. Belton 1994. HST observations of Chiron's inner coma–A possible bound atmosphere? *Bull. Am. Astron. Soc.* **26,** 1152–1153.

Olkin, C. B., and J. L. Elliot 1994. Occultation astrometry: Predictions and post-event results. In *Galactic and Solar System Optical Astrometry* (L. V. Morrison and G. F. Gilmore, Eds.), pp. 286–290. Cambridge Univ. Press, Cambridge.

Stellingwerf, R. F. 1978. Period determination using phase dispersion minimization. *Astrophys. J.* **224,** 953–960.

Stern, S. A., A. A. Jackson, and D. C. Boice 1994. Numerical simulations of particle orbits around 2060 Chiron. *Astron. J.* **107,** 765–771.

Sykes, M. V., and R. G. Walker 1991. Constraints on the diameter and albedo of 2060 Chiron. *Science* **251,** 777–780.

Sykes, M. V., and R. G. Walker 1992. Cometary dust trails. I. Survey. *Icarus* **95,** 180–210.

Thomas, P. C. 1989. The shapes of small satellites. *Icarus* **77,** 248–274.

West, R. M. 1991. A photometric study of (2060) Chiron and its coma. *Astron. Astrophys.* **241,** 635–645.

Womack, M., and S. A. Stern 1995. Detection of carbon monoxide in (2060) Chiron. *Bull. Am. Astron. Soc.* **27,** 1143.